Published in final edited form as:
Cancer Cell. 2012 May 25; 21(5): 601–613. doi:10.1016/j.ccr.2012.04.012.

Distinct Neural Stem Cell Populations Give Rise to Disparate Brain Tumors in Response to N-MYC

Fredrik J. Swartling[1,2,*], **Vasil Savov**[2,**], **Anders I. Persson**[1,**], **Justin Chen**[1], **Christopher S. Hackett**[1], **Paul A. Northcott**[3], **Matthew R. Grimmer**[1], **Jasmine Lau**[1], **Louis Chesler**[4], **Arie Perry**[1], **Joanna J. Phillips**[1], **Michael D. Taylor**[3], and **William A. Weiss**[1,*]

[1]University of California, Depts. of Neurology, Pathology, Pediatrics, Neurosurgery, Brain Tumor Research Center and Helen Diller Family Comprehensive Cancer Center, San Francisco CA 94158, USA

[2]Department of Immunology, Genetics and Pathology, Rudbeck Laboratory, Uppsala University, Uppsala, Sweden

[3]The Hospital for Sick Children, Toronto, Ontario, M5G 1X8, Canada

[4]The Institute of Cancer Research, Sutton, Surrey, SM2, 5NG, United Kingdom

SUMMARY

The proto-oncogene *MYCN* is mis-expressed in various types of human brain tumors. To clarify how developmental and regional differences influence transformation, we transduced wild-type or mutationally-stabilized murine *N-myc*^{T58A} into neural stem cells (NSCs) from perinatal murine cerebellum, brain stem and forebrain. Transplantation of *N-myc*^{WT} NSCs was insufficient for tumor formation. *N-myc*^{T58A} cerebellar and brain stem NSCs generated medulloblastoma/primitive neuroectodermal tumors, whereas forebrain NSCs developed diffuse glioma. Expression analyses distinguished tumors generated from these different regions, with tumors from embryonic versus postnatal cerebellar NSCs demonstrating SHH-dependence and SHH-independence, respectively. These differences were regulated in-part by the transcription factor SOX9, activated in the SHH subclass of human medulloblastoma. Our results demonstrate context-dependent transformation of NSCs in response to a common oncogenic signal.

Keywords

N-MYC; GFAP; SOX9; medulloblastoma; neural stem cells; glioma

*Corresponding authors: waweiss@gmail.com, Phone/Fax: +1-(415)-502-1694/+1-(415)-476-0133 and fredrik.swartling@igp.uu.se, Phone/Fax: +46-(18)-471-4831/+46-(18)-55-8931.
**Equal contribution.

ACCESSION NUMBERS

Microarray data have been deposited in the GEO public database (http://www.ncbi.nlm.nih.gov/geo/), with accession number GSE36594.

SUPPLEMENTAL INFORMATION

Supplemental information includes eight figures, three tables, supplemental experimental procedures and supplemental references.

The authors declare no conflict of interest.

INTRODUCTION

Medulloblastoma (MB), the most common malignant primary brain tumor of childhood, arises in the cerebellum. Classic, desmoplastic (nodular) and large cell/anaplastic (LC/A) pathologies are described (Eberhart et al., 2004) and transcriptional profiling has identified distinct subgroups characterized by signaling through WNT, SHH or other signaling pathways that include MYC and MYCN (Taylor et al., 2011). Activation of SHH signaling occurs in ~25% of tumors (Browd et al., 2006; Kessler et al., 2009; Polkinghorn and Tarbell, 2007). Patients with WNT-driven tumors show a favorable outcome when compared with SHH-driven tumors, while tumors of transcriptomal groups 3 and 4 have the worst outcomes (Eberhart et al., 2004; Ellison et al., 2011; Pfister et al., 2009; Polkinghorn and Tarbell, 2007).

Amplification of *MYC* and *MYCN* occurs in ~10% of MB, associated with aggressive LC/A tumors and poor survival. Expression of MYCN is high in SHH-driven human tumors, and murine N-MYC can potentiate preclinical models of MB driven by activated SHH signaling. In contrast, MYCN-amplified tumors are predominantly of non-SHH MB subtypes (Korshunov et al., 2011); and mis-expression of MYCN occurs in the majority of MB in all histopathologies (Northcott et al., 2009; Pomeroy et al., 2002; Swartling et al., 2010). Neither gain nor mis-expression of *MYCN* is exclusive to MB, as *MYCN* is also amplified and/or mis-expressed in malignant glioma, the most common primary brain tumor of adults, and typically localized to forebrain (cerebrum) rather than hindbrain (cerebellum) (Brennan et al., 2009; Hui et al., 2001; Perry et al., 2009).

The cell of origin for both MB and glioma is debated. One candidate is the neural stem cell (NSC) with self-renewal capacity and potential to generate progenitors and differentiated cells of all neural lineages. NSCs can be derived from either cerebellum or cerebrum both during development and in adulthood (Lee et al., 2005; Reynolds and Weiss, 1992). During both normal cerebellar development and MB tumorigenesis, N-MYC drives proliferation of granule neuron precursors (GNPs). GNPs are marked by transcription factors including MATH1 and PAX6, and are derived from radial glia or NSCs of the developing cerebellum (Hatton et al., 2006; Knoepfler et al., 2002; Lin et al., 2001; Schuller et al., 2008; Yang et al., 2008). Constitutive deletion of *N-myc* is embryonic lethal (Charron et al., 1992; Stanton et al., 1992) while inactivation in NSCs leads to thinning of the NSC-rich ventricular zone (VZ), a markedly reduced cortex, and a diminutive cerebellum (Knoepfler et al., 2002). These results indicate a role for N-MYC in regulating normal forebrain and hindbrain development.

To understand whether changes in normal developmental programs could influence transformation, we transduced *N-myc* into forebrain, cerebellar or brain stem tissues isolated at distinct developmental time points. We studied mechanisms for tumor development and compared expression profiles among the disparate brain tumors generated by this common oncogene. In the analysis we included our recently described murine MYCN-driven MB model in which the Glutamate Transporter 1 (GLT1) promoter drove a bidirectional Tetracycline-Response Element (TRE), directing expression of *MYCN* and Luciferase (GTML) (Swartling et al., 2010).

RESULTS

MB spheres are MYCN-dependent and express neuronal markers

We isolated brain tumors from nine mice from the transgenic GTML model, and derived tumor spheres in neurobasal (NB) media supplemented with EGF and FGF. Eight representative sphere lines, GTML2-9, arose independently of SHH (Swartling et al., 2010),

and showed elevated expression of MYCN protein and Luciferase (LUC) (Figure 1A and Figure S1A). SHH-dependent GTML tumors arise at < 5% frequency. A single line (GTML1) was isolated from a SHH-dependent GTML tumor and showed low levels of MYCN mRNA (described previously as GTML-T7 (Swartling et al., 2010)). While MYCN-low GTML1 cells showed no response to doxycycline (dox), proliferation of MYCN-high GTML spheres was blocked after 3–5 days of dox treatment, reflecting MYCN-dependence (Figs 1B and 1C, Figures S1B–S1D). This proliferation block, associated with loss of Cyclin D2, did not recover after dox wash out, as compared to controls (Figures S1D and data not shown). These observations are consistent with our earlier in-vivo observations in GMTL mice that withdrawal of MYCN in tumors led to senescence (Swartling et al., 2010).

To confirm SHH-independence of MYCN-positive GTML2-9 tumor spheres, we cultured spheres with the SMO inhibitor cyclopamine (Taipale et al., 2000), which blocks signaling downstream from SHH. GTML1 SHH-dependent spheres responded to SMO inhibition. However, no significant differences in proliferation were observed after treating GTML2-9 spheres with cyclopamine (Figures 1D and 1E and data not shown), or with SHH-N or SMO agonists that activate SHH signaling (not shown). These data are consistent with tumors arising through a SHH-independent pathway. However, it remains possible that signaling downstream of SMO could contribute to tumor formation.

Compared to WT cerebellar spheres and SHH-dependent GTML1 spheres, GTML2-4 tumor spheres with high levels of MYCN protein showed elevated levels of mRNA for *Ngn1* and *Syp* (Figure 1F–1G). NGN1, an inducer of neurogenesis and a marker of immature GABAergic cells originating from the roof of the fourth ventricle, is typically expressed in MATH1-negative, classic MB (Farah et al., 2000; Salsano et al., 2007). Spheres from GTML 2-4 showed low levels of glial-lineage transcription factors *Olig2* and *Sox9* (Figures 1H and 1I), both of which are also typically low in human MB, and high in cultured normal human cerebellar NSCs (Alcock and Sottile, 2009; de Bont et al., 2008; Ligon et al., 2004). These marker data collectively verify that GTML2-4 spheres resemble SHH-negative human MB.

Freshly isolated GTML tumor cells can be transplanted orthotopically into the brains of immunocompromised mice to regenerate MB (Swartling et al., 2010). While SHH dependent GTML1 tumor spheres did not grow orthotopically, spheres from SHH independent tumors (GTML2 and GTML3) generated lethal tumors (Figure S1E). Transplanted GTML2 tumor spheres grew significantly more rapidly than transplanted GTML3 tumor spheres consistent with higher levels of MYCN protein in GTML2 cells (Figures S1D and S1E).

To determine whether NSCs isolated from normal cerebellum could represent cells of origin for GTML MB, we crossed Glt1-tTA mice to TRE-Cre:Rosa26-lsl-LacZ reporter animals, enabling us to visualize LacZ as a marker of cell fate. Indeed, NSCs cultured as spheres from these triply transgenic mice at postnatal ages were β-galactosidase-positive suggesting that the GLT1 promoter is active and that GTML tumors could originate from normal NSCs (Figures 1J and 1K).

Transduction of *N-myc*^{T58A} into the GFAP-positive NSCs boosts proliferation

GFAP is a stem cell and astroglial marker (Doetsch et al., 1999) and shows tight co-expression with GLT1 both in cerebellar and cerebral cells in vivo (Schmitt et al., 1996) as well as in our NSC cultures (Figure S1F). We therefore investigated how GFAP-positive populations of NSCs would respond to *N-myc*, using mice transgenic for the avian *tv-a* retroviral receptor driven by the GFAP promoter (*Gtv-a*) (Holland et al., 2000). We dissected cells at embryonic day 16 (E16) and postnatal day 0 (P0) from three different brain

regions of *Gtv-a* mice (Figure 2A): luminal parts of forebrain ventricular zone (< 1 mm), total cerebellum, and the top layer (< 1 mm) isolated from the ventricular zone region of the dorsal brain stem. This isolated region encompassed both VZ brain stem cells and the lower rhombic lip (LRL) structure that contains candidate cells of origin for MB (Gibson et al., 2010).

Dissected cells were cultured in neurobasal media for one week and subsequently transduced with harvested RCAS viruses containing either a GFP reporter, Flag-tagged wild-type *N-myc*^{WT}, or mutationally-stabilized Flag-tagged *N-myc*^{T58A} (Figure S2A–E). After differentiation for 72h without growth factors, most GFP-transduced NSCs from both E16 and P0 cerebellar and forebrain NSCs remained positive for the NSC marker GFAP, but were negative for the neuronal marker, TUJ1, confirming selective transduction of GFAP-positive NSCs (Figures 2B and S2F).

To further characterize the types of cells transduced, we sorted GFP-positive and negative NSC fractions from E16 cerebellum, and P0 cerebellum and forebrain, 72h after transduction with RCAS-GFP. The percentage of GFP-positive cells ranged from 2.5% up to 8% of the entire cell population (Figures 2B and S2F). Interestingly, GFP-sorted single NSCs from these conditions produced significantly more secondary spheres than GFP-negative NSCs after two weeks in culture (Figure S2G). These data are consistent with selective transduction of GFAP-positive cells within these primary cultures, showing increased self-renewal as compared with more differentiated populations of cells.

We next analyzed cells transduced with RCAS-*N-myc* constructs. *N-myc*^{T58A}-transduced cerebellar NSCs stained intensely for Flag on Western Blot as compared to *N-myc*^{WT}-transduced cells (Figure 2C), likely reflecting stabilization of N-MYC protein due to decreased proteasomal degradation (Salghetti et al., 1999). As compared to cerebellar NSCs transduced with GFP or *N-myc*^{WT}, NSCs transduced with *N-myc*^{T58A} and GTML2 tumor spheres were both resistant to blockade of new protein synthesis by cycloheximide (CHX, Figures S2H–S2K) consistent with stabilization of N-MYC^{T58A} or overexpression of MYCN in these cells.

While GFP- and *N-myc*^{WT}-transduced NSCs showed moderate proliferation when cultured on coated plates, transduction of *N-myc*^{T58A} into NSCs from P0 cerebellum promoted increased proliferation, associated with high levels of the fourth ventricular zone marker NGN1 (Figures 2C and 2D). Similarly, transduction of *N-myc*^{T58A} into P0 forebrain NSCs, as well as E16 NSCs from both cerebellum and forebrain, promoted proliferation, as compared to both vector GFP control and *N-myc*^{WT}-transduced NSCs (Figure 2E and not shown).

Because NSCs in the brain stem may also generate brain tumors (Gibson et al., 2010), we next tested VZ-derived NSCs from dorsal brain stem. *N-myc*^{T58A} did not clearly drive increased proliferation in E16 and P0 brain stem cultures in this system (not shown), prompting us to test VZ-derived NSCs from E14 dorsal brain stem/LRL (henceforth called E14 LRL). Transduction of E14 LRL NSCs cells with *N-myc*^{T58A} led to increased proliferation as compared to GFP- and *N-myc*^{WT}-transduced NSCs (Figure 2F).

Culturing cerebellar NSC for a week in neurobasal media typically removes any residual GNPs (Klein et al., 2005; Sutter et al., 2010). Transduction of *N-myc*^{WT} or *N-myc*^{T58A} retroviruses into purified P0 GNPs did not drive proliferation, presumably because very few PAX6 positive GNPs also expressed GFAP and tv-a, thus evading viral transduction (Figures S2L–S2M).

To clarify whether *N-myc* could drive self-renewal and substitute for growth factors, we cultured NSCs and tumor spheres in limiting dilution for one week with or without EGF and FGF (10 cells/well). To distinguish effects on NSCs from effects on neural progenitors, 100 cells/well were re-plated in a secondary sphere formation assay for a second week. *N-myc*^{WT}-, *N-myc*^{T58A}- and GFP-transduced control secondary spheres retained strict growth factor dependence and showed no significant differences in sphere number (Figures 2G–2I, Figures S2N–S2P). By contrast, GTML tumor spheres generated secondary spheres even when cultured without growth factors (Figure 2J). MYCN blocked differentiation in GTML tumor spheres, as spheres with high MYCN protein levels neither differentiated nor extended processes upon growth factor starvation or doxycycline treatments (not shown). In contrast and as expected, SHH-dependent GTML1 cells and control cerebellar NSCs transduced with GFP virus showed multipotent differentiation into both GFAP-positive astrocytes and TUJ1-positive neurons (Figures 2B, S2F and not shown).

An N-MYC neuronal program depends on both developmental age and regional origin

To characterize the potential for *N-myc* to induce distinct differentiation programs as a function of both NSC age and regional origin, we analyzed the glial markers SOX9 (Stolt et al., 2003) and GFAP, 72 hours after transduction of *N-myc*^{T58A} into cerebellar NSCs at E16 and P0 and forebrain NSCs at P0. *N-myc*^{T58A}-transduced NSCs all showed increased N-myc mRNA levels as by Affymetrix exon array analysis of distinct NSC populations. P0 cerebellar NSCs transduced with *N-myc*^{T58A} showed reduced mRNA expression of Gfap and protein levels of SOX9 as compared to E16 cerebellar NSCs; whereas P0 forebrain NSCs showed elevated levels of Gfap and SOX9 (Figure 3A).

As SOX9 has been reported to also act downstream of the SHH/SMO to induce and maintain NSCs (Scott et al., 2010), we next asked whether *N-myc*^{T58A} affected SHH signaling. GFP-transduced control NSCs from E16 and P0 cerebellum and forebrain all responded to SMO inhibition through cyclopamine treatment (Figures 3B and 3C), consistent with reports that forebrain NSCs, cerebellar radial glia, and cerebellar NSCs are sensitive to SHH signals in vivo (Ahn and Joyner, 2005; Huang et al., 2010). While *N-myc*^{T58A}-transduced E16 cerebellar cells and *N-myc*^{T58A}-transduced P0 forebrain cells retained sensitivity to cyclopamine, *N-myc*^{T58A}-transduced P0 cerebellar and E16 forebrain cells, like GTML tumor spheres, were resistant (Figures 3D and 3E).

In comparing cyclopamine sensitive and resistant *N-myc*^{T58A}-transduced cerebellar cultures, we again used Affymetrix exon arrays to analyze expression of Smo, a co-receptor for the SHH signal; Sfrp1, a marker of SHH-driven MB; Gli1, a marker of SHH activation, and Gli3, a marker of SHH repression. Expression of Smo was unchanged in comparing P0 and E16 cultures (Figures S3A and S3B). Cyclopamine-resistant P0 cultures showed repression of SHH signaling. Both Sfrp1 and Gli1 were decreased, while Gli3 was upregulated in P0 *N-myc*^{T58A} cultures, as compared to E16 cerebellar NSCs. Collectively, these studies demonstrate that *N-myc*^{T58A} promotes SHH independence (downstream of SMO) in postnatal cerebellar cells, in embryonic forebrain cells, and in GTML tumors.

N-myc^{T58A} initiates brain tumors from NSCs

To clarify whether N-MYC could induce brain tumors from NSCs, and whether the differentiative programs shown in Figure 3 would persist in vivo, we transduced embryonic and postnatal NSCs with *N-myc*^{WT} or *N-myc*^{T58A} and transplanted cells orthotopically into the brains of nude mice. In contrast to *N-myc*^{WT} NSCs, *N-myc*^{T58A} NSCs from E16 and P0 cerebellum or E16 and P0 forebrain all formed brain tumors (Figures 4A and 4B). *N-myc*^{T58A} cerebellar NSCs generated tumors at higher incidence and penetrance than the *N-myc*^{T58A} forebrain NSCs (Figures 4A and 4B). We also analyzed LRL-derived NSC.

Consistent with our *in-vitro* data, *N-myc*^{T58A} E16 and P0 LRL NSCs failed to generate brain tumors, while *N-myc*^{T58A} –transduced E14 LRL NSCs generated brain tumors in 40% of mice when transplanted orthotopically (Figure 4C).

Orthotopic transplantation of *N-myc*^{T58A} P0 cerebellar NSCs into cerebellum resulted in massive tumors with morphology of human MB, including Homer Wright (neuroblastic) rosettes, and prominent cell wrapping characteristic of LC/A tumors (Figures 4D, 4E and Figure S4A)). The histology of *N-myc*^{T58A} P0 cerebellar tumors also resembled GTML tumors (Swartling et al., 2010), sometimes showing LC/A histopathology (Figures S4B–S4C). Similarly, orthotopic transplantation of *N-myc*^{T58A} P0 forebrain NSCs into cerebrum induced aggressive forebrain tumors (Figure 4F) that were more invasive than the cerebellar tumors (Figure 4G). The P0 forebrain tumors resembled diffuse gliomas in terms of distant spread of individual tumor cells along white matter tracts (Figure 4G and S4D). E14 LRL tumors were typically characterized by marked cellular and nuclear pleomorphism (Figure 4H–I).

While no differences in proliferation (KI67) and vascularity (CD34) were found among the P0 forebrain and P0 cerebellar tumors, P0 cerebellar tumors were significantly more apoptotic than P0 forebrain tumors (Figures S4E–S4J). P0 cerebellar tumors were generally negative or showed only scattered cells positive for the astrocytic markers GFAP, OLIG2, and SOX9 (Figures 4J–4L) and moderate immunoreactivity for the neuronal marker SYP (Figure 4M). In contrast, P0 forebrain tumor cells were strongly positive for GFAP, OLIG2 and SOX9 (Figures 4N–4P) and negative for SYP (Figure 4Q). LRL tumors showed an intermediate phenotype with few scattered cells positive for the astrocytic markers GFAP, moderate positivity for OLIG2 and SOX9 (Figures 4R–4T) and scattered islands of SYP positive cells (Figure 4U).

The histology of *N-myc*^{T58A} tumors induced from E16 cerebellar, E16 forebrain NSCs generally resembled *N-myc*^{T58A} tumors induced from P0 cerebellar and P0 forebrain NSCs, respectively (Figures S4K and S4L). The majority of tumors derived from E16 cerebellar NSCs were SOX9 positive (Figure S4M). Most embryonic forebrain tumors showed distinct areas of glial differentiation (Figure S4N). Lack of nuclear β-catenin expression in LRL tumors (Figure S4O) suggests a WNT-independent tumor subtype, as compared to a recently reported model for MB also derived from LRL cells originating from brainstem (Gibson et al., 2010). These and tumors from E16 or P0 cerebellum were similarly insensitive to the GSK3β inhibitor TWS119 at 1μM (not shown) demonstrating WNT-independence, although it remains possible that *N-myc*^{T58A} affects the ability of GSK3β to phosphorylate and destabilize β-catenin.

Regional origin exerts a dominant effect on brain tumor type

Transplantation of normal cerebellar NSCs into forebrain VZ generates mostly GFAP-positive astroglial cells (Klein et al., 2005). To determine if the regional brain niche was responsible for the generated tumor phenotypes we injected *N-myc*^{T58A} –transduced P0 cerebellar NSCs into the forebrain and *N-myc*^{T58A} –transduced P0 forebrain NSCs into the hindbrain. We studied the same markers as in Figure 4 and quantified positive cells (Table S1). We included three controls each of site-matched tumors for E16 and P0 cerebellum, tumors from E16 forebrain, P0 forebrain and E14 brain stem; and three GTML tumors.

For all tumors, we also examined protein expression of KCNA1, a Kv1.1 voltage-gated potassium channel-encoding gene associated with Group 4 MB (Taylor et al., 2011) as well as the LRL and WNT markers OLIG3 and β-catenin, respectively (Gibson et al., 2010). The profiles of GFAP, Nestin and SYP in tumors correlated generally with region from which NSCs were isolated, rather than region of the brain into which we injected transduced cells.

Like the LRL tumors (Figure S4O), all tumors examined were negative for nuclear β-catenin (Table S1). Intriguingly, SOX9 and OLIG2 showed a modest and differential expression pattern in "misplaced" tumors, with higher levels of protein expression in misplaced hindbrain tumors and lower expression levels in misplaced forebrain tumors (Table S1). Our data still suggests that region of origin exerts a dominant effect on tumor type.

SOX9 marks SHH-dependent MB and malignant glioma

Transduction of *N-myc*^{T58A} into murine NSCs led to regional and age-dependent changes in levels of SOX9 protein (Figure 3A). To further clarify the expression of SOX9 in MB, we analyzed array data from 103 human MBs segregated into WNT, SHH, Group 3 or Group 4 tumors (Northcott et al., 2011; Taylor et al., 2011). Clustering and expression patterns were consistent with both SOX9 and MYCN as markers for WNT- and SHH-driven human tumors (Figure 5A). NGN1 expression was increased in all subtypes except for the SHH group, marked by the human MATH1 ortholog, ATOH1, and supported by previous data discriminating these subclasses (Cho et al., 2011; Kool et al., 2008; Northcott et al., 2011; Thompson et al., 2006). Consistent with the findings of SOX9 as a marker of SHH-driven tumors, levels of SOX9 levels were highest in infant and adult MB patients (Figure S5), which are typically SHH-dependent (Northcott et al., 2011). Furthermore, SOX9 was only observed in a few scattered cells in a representative human classic MB (Perry et al., 2009) previously reported to lack *MYCN* amplification (Figure 5B), while a human *MYCN*-amplified MB showed high levels of SOX9 (Figure 5C).

The pathology and marker-expression in P0 forebrain tumors is characteristic of aggressive human malignant glioma with components of primitive neuroectodermal tumors (MG-PNET). We recently described 53 cases of human MG-PNET, detailing both poor survival (essentially identical to human high-grade glioma) and common amplification of *MYC* and *MYCN* (43%) in PNET-like foci (Perry et al., 2009). Since MG-PNET may arise in the setting of relapsed glioblastoma (GBM), we next analyzed data from The Cancer Genome Atlas (TCGA) (2008). While OLIG2 and SOX9 were overexpressed in half or more than half of the GBM samples, expression of neuronal markers like NGN1 and SYP were downregulated in most samples (Table S2). Among 424 human GBMs, 20% overexpressed MYCN, consistent with a role for *MYCN* in the pathogenesis of some GBMs (Table S2). Irrespective of MYCN amplification, human MG-PNET samples showed high level and distinct nuclear expression of SOX9 (Figures 5D and 5E), consistent with results from glioma cell lines (Swartling et al., 2009) and TCGA data (Table S2).

Alignment of murine tumors and classification using human MB subgroup identifiers

Having demonstrated that SOX9 can mark SHH-driven human MB, we next applied these observations to murine *N-myc*^{T58A} MB and GTML tumors, using Affymetrix exon arrays. Unsupervised clustering revealed that *N-myc*^{T58A} tumors from E16 cerebellum, P0 cerebellum and P0 forebrain NSCs were closely aligned to the NSCs from which they were derived (Figure 6). *N-myc*^{T58A} tumors and their corresponding NSCs were more similar to GTML tumors than to normal cerebellum (Figure 6). Within the *N-myc*^{T58A} tumor group, the region of origin (cerebellum vs forebrain) was a larger separator than the age of isolation of the initiating cells. Originating NSCs, *N-myc*^{T58A} tumors, and GTML tumors were all more similar to each other than to normal cerebellum. The signature of NSCs vs tumor was greater than the difference between NSC types, precluding the use of gene expression signatures to identify the most similar potential originating cell.

Using identifiers for subtypes of human MB (Northcott et al., 2011), E16 MB (generated from *N-myc*^{T58A}-transduced E16 cerebellar NSCs) showed a distinct SHH-pathway profile (Figure S6A) while both P0 MB (generated from *N-myc*^{T58A}-transduced P0 cerebellar

NSCs) and GTML tumors presented significantly higher expression of the Group 4 identifier KCNA1, as compared to E16 MB. By contrast, the other subgroup identifiers, DKK1 (WNT), SFRP1 (SHH), and NPR3 (Group 3), did not significantly delineate these groups (Figure S6B).

E16 *N-myc^{T58A}* cerebellar tumors model SHH-dependent MB, while P0 tumors model SHH-independent disease

Expression levels of Sox9, N-myc and Math1 further distinguished the various *N-myc^{T58A}* tumors using both Affymetrix arrays as well as real-time qPCR, as compared to expression levels in adult cerebellum (Figures 7A–7C and Figure S7A and S7B). E16 MB showed high levels of Sox9 mRNA, N-myc, and of the EGL marker Math1 suggesting a SHH- rather than a WNT-dependent subtype (Figures 7A–7C). In contrast, P0 MB displayed lower expression of Sox9, N-myc and Math1. Similar to P0 MB, E14 LRL tumors (generated from *N-myc^{T58A}*-transduced prenatal LRL NSCs) showed low N-myc and Math1 levels consistent with a SHH-independent origin (Figures 7A–7C).

Interestingly, forebrain *N-myc^{T58A}* P0 tumors (P0 glioma) showed high levels of Sox9 and N-myc and absent Math1 (Figures 7A–7C), consistent with transformation of a forebrain cell type that shows SHH-dependence independently of Math1 (Akazawa et al., 1995). Expression analysis substantiated the glioma phenotype observed in the forebrain tumors, in which levels of Gfap were significantly elevated as compared to hindbrain tumors (Figure S7B). Moreover, Nestin (*Nes*) was among the top 30 genes overexpressed in P0 glioma as compared to P0 MB (Table S3). P0 MB showed a low immunoreactivity of Nestin while P0 glioma showed elevated Nestin expression (Figure S7C–D and Table S1). As Nestin is a strong marker for glioma and upregulated in 99% of human GBM samples in the TCGA database (Table S2), increased Nestin expression suggests a glioma-like differentiation pattern in forebrain tumors compared to the MB-like pattern seen in cerebellar tumors.

In agreement with SOX9 as a marker for SHH-dependence, cultured P0 MB spheres with low levels of SOX9 were resistant to cyclopamine (Figure 7D). Conversely, both E16 MB and P0 glioma with high SOX9 levels were cyclopamine-sensitive (Figure 7D). Similar dependence on SHH was also observed in *N-myc^{T58A}* NSCs prior to orthotopic implantation and tumor formation (Figures 3B–E). These results suggest that *N-myc^{T58A}* initiates SHH-dependent transformation in both E16 cerebellar NSCs and P0 forebrain NSCs, while transformation of E16 forebrain NSCs and P0 cerebellar NSCs (and possibly in brain stem NSCs) occurs through a SHH-independent pathway.

SOX9 promotes self-renewal and generates GLI2-expressing tumors at shorter latency

Our data demonstrates that P0 MBs arise through a SOX9- and SHH- independent program. To establish whether SOX9 plays a functional role in transforming P0 cerebellar NSCs, we generated *SOX9* RCAS viruses (Figure S8A) and selectively transduced *Gtv-a* positive P0 *N-myc^{T58A}* cerebellar NSCs or P0 MB spheres (isolated from individual P0 MBs). Forced expression of SOX9 suppressed proliferation in P0 *N-myc^{T58A}* cerebellar cells and in P0 MB spheres (Figure S8B), which have low levels of SOX9 (Figures 3A, 4I and 7A). In contrast, similar forced expression of SOX9 did not affect E16 MB and P0 glioma, which have high SOX9 levels at baseline (Figures S8C–D).

Although forced expression of SOX9 suppressed proliferation in *N-myc^{T58A}* cerebellar cells and in P0 MB spheres, SOX9 actually drove increased self-renewal when culturing these at a limited dilution. Single cell clones from normal P0 cerebellar NSCs and P0 cerebellar NSCs transduced with *N-myc^{T58A}* were transduced with SOX9, and clones with high levels of SOX9 were selected (Figure 8A). SOX9 increased self-renewal in both normal and *N-*

myc^{T58A} –transduced P0 cerebellar NSC clones, as compared to normal and *N-myc*^{T58A} –transduced P0 cerebellar NSC clones without forced expression of SOX9 (Figure 8B). Single cell spheres and spheres generated from an isolated P0 MB (P0C-T3, also cultured and propagated from a single cell clone) were dependent on growth factors EGF and FGF as compared to single cell clones subcloned out from the GTML2 sphere line (Figure 1A) that generated secondary spheres essentially independently of growth factors. Forced expression of SOX9 was also associated with higher levels of Gli2 (Figure 8C–E) suggesting that SOX9 can drive SHH-signaling in these cells.

Since forced expression of SOX9 drove self-renewal while blocking proliferation of cells in-vitro, we next asked how these potentially opposing activities would impact tumor formation in vivo. Forced expression of SOX9 and *N-myc*^{T58A} in P0 cerebellar NSCs generated orthotopic tumors at shorter latency and with increased tumor penetrance, as compared with NSCs expressing *N-myc*^{T58A} alone (Figure 8F). The SOX9 expressing tumor cells demonstrated marked cellular and nuclear pleomorphism, numerous mitoses, and numerous apoptotic bodies, consistent with a primitive neuroectodermal phenotype (Figure S8E). Focally tumor cells contained abundant cytoplasm and GFAP-immunostaining demonstrated a population of GFAP-positive tumor cells. (Figures S8E and S8F). These observations suggest that SOX9 can cooperate with N-MYC to promote malignant progression acting upstream of GLI2.

Forced expression of *N-myc*^{T58A} repressed SOX9 in P0 cerebellar NSCs. Is SOX9 similarly repressed in GTML tumors? In response to dox-mediated withdrawal of MYCN, some cells within GTML tumors undergo senescence (Swartling et al., 2010). Consistent with this result, dox-treatment of GTML3 tumor spheres led to death of most cells, while a few cells remained viable without proliferating (Figures S8G-S8H and data not shown). In response to withdrawal of MYCN, these viable cells showed elevated levels of SOX9 at levels similar to SHH-dependent GTML1 control cells (Figure 8G). This suggests SOX9 is repressed by forced expression of MYCN also in SHH-independent GTML tumors. Collectively, data in Figure 8 demonstrate that interactions between N-MYC and SOX9 regulate proliferation, differentiation, and self-renewal in P0 *N-myc*^{T58A}MB, and that similar interactions are relevant to *MYCN*-driven GTML MB.

DISCUSSION

Deletion of *N-myc* in neural stem and progenitor cells in the mouse causes reduced cellularity of both forebrain and hindbrain, suggesting an essential role in the growth and development of these structures (Knoepfler et al., 2002). Here, by orthotopic transplantation of *N-myc*^{T58A} NSCs, we validate a reciprocal role for mis-expression of *N-myc* in the pathogenesis of both forebrain and hindbrain tumors. Our data, and the finding that *MYCN* is commonly over-expressed in both forebrain and in hindbrain tumors in humans (Brennan et al., 2009; Eberhart et al., 2004; Hui et al., 2001; Perry et al., 2009; Pfister et al., 2009; Pomeroy et al., 2002) suggest a role for *MYCN* in the development of brain tumors.

Our experiments are consistent with recent results suggesting a relationship between normal NSCs and tumor initiating cells (Holland et al., 2000; Johnson et al., 2010; Schuller et al., 2008; Sutter et al., 2010; Yang et al., 2008). Orthotopic injection of *N-myc*^{T58A} DF-1 virus-producing cells failed to generate brain tumors ((Browd et al., 2006) and our unpublished data), perhaps in part because few, if any, NSCs are successfully transduced through this approach. We instead generated five different tumors from distinct NSCs transduced with *N-myc*^{T58A} after a brief propagation in culture. *N-myc*^{T58A} NSCs derived from embryonic cerebellum led to SHH-dependent MB, consistent with transduction of a GFAP-positive NSC with a propensity to become a MATH1-positive granule neuron precursor (Marino et

al., 2000; Schuller et al., 2008; Yang et al., 2008). In contrast, *N-myc*^{T58A} NSCs derived from postnatal forebrain led to tumors with characteristics of malignant glioma, consistent with transduction of a GFAP-positive NSC with a propensity to become a MATH1-negative, SHH-dependent forebrain cell (Palma et al., 2005).

N-myc^{T58A} NSCs derived from embryonic forebrain generated brain tumors at low penetrance. Analysis of a limited number of these tumors suggests transduction of a GFAP-positive NSC with a propensity to become a SHH-independent forebrain glioma. *N-myc*^{T58A} NSCs derived from postnatal cerebellum led to SHH-independent MB with low levels of Math1 and Sox9. Tumors were also generated from the lower rhombic lip or the dorsal regions of the VZ of the developing brain stem. Interestingly, only E14 LRL NSCs could induce brain tumors, whereas no tumors were observed from E16 or PO LRL/brain stem NSCs.

That our LRL tumors were only seen at E14 ages correlate with previous findings of WNT-subtype MB in the murine LRL/dorsal brainstem generated between E11.5 and E15.5 (Gibson et al., 2010). Our LRL tumors resembled human anaplastic MB/PNETs and arose independently of WNT signaling, with negative immunoreactivity for nuclear β-catenin and the LRL marker OLIG3. These tumors might thus arise from a brain stem VZ cell type distinct from an OLIG3-positive LRL progenitor (Storm et al., 2009). LRL tumors lacked Math1 expression, and showed moderate levels of Sox9. The low levels of Math1 are also characteristic of GTML MB arising in transgenic mice, and are consistent with transduction of a GFAP/GLT1 double positive NSC with potential to become a MATH1-negative, SHH-independent progenitor.

Expression analysis of E16 MB revealed elevated levels of many genes upregulated in the SHH subclass of human MB; while both P0 MB and GTML MB were at least somewhat aligned with human Group 4 MB (Taylor et al., 2011). Collectively, our experiments argue that GFAP-positive NSCs from forebrain and hindbrain can give rise to both malignant glioma and to at least two distinct subtypes of MB, a SHH subgroup and a SHH-independent Group 4 MB subgroup, together representing 38% and 62% of MYCN-amplified human MB, respectively (Korshunov et al., 2011). We have not demonstrated that the cells of origin for our tumors truly represent self-renewing tripotent NSCs. Therefore, it remains possible that the cells we refer to as NSCs, actually represent progenitors with a more limited potential for differentiation. In either case, our observations raise questions as to the nature of cells transformed in human tumors. If mutations that contribute to transformation occur in NSCs (or progenitors) during embryonic or postnatal ages, then rests of partially transformed NCSs or of glial progenitors derived from these cells, might persist into childhood or even adulthood, later giving rise to tumors.

SOX9 acts downstream of SHH signaling, at least in part because GLI1, a marker of SHH activation, binds directly to a regulatory element in the *SOX9* promoter region, driving expression (Bagheri-Fam et al., 2006; Vidal et al., 2005). SOX9 is essential for formation and maintenance of multipotent NSCs and is an effector of SHH signaling (Scott et al., 2010). SOX9 levels were high in *SHH*-driven human MB, a finding aligned with our murine data that E16 cerebellar NSCs retain SOX9 expression upon transformation, and respond to SHH inhibition. Forced expression of SOX9 in P0 *N-myc*^{T58A} cerebellar NSCs showed that SOX9 antagonized proliferation driven by *N-myc*^{T58A} in P0 tumors. However, SOX9 also promoted self-renewal, associated with increased expression of Gli2 in P0 *N-myc*^{T58A} cerebellar NSCs, leading to increased penetrance of a Gli2-expressing tumor. These data demonstrate that SOX9 expression can promote SHH-activation in *N-myc*^{T58A} MB, and suggest SOX9 as an important regulator of SHH MB. Further, our observations are consistent with a model in which N-MYC promotes a neuronal fate in P0 cerebellar NSCs,

associated with repression of SOX9 and expression of neuronal markers like NGN1, resulting in a profile similar to the majority of human MB.

N-myc^{T58A} forebrain tumors showed significant glial differentiation without microvascular proliferation, pseudopalisading cells and necrosis. These features are reminiscent of human MG-PNET, a tumor type that we recently detailed, and which shows frequent amplification of *MYCN* (Perry et al., 2009). The association of *MYCN* amplification with MG-PNET and our ability to model these tumors in the mouse collectively support a role for *MYCN* in the pathogenesis of malignant glioma. Since MG-PNET may arise in the setting of pre-existing or recurrent GBM (Perry et al., 2009) our studies also provide a mouse model both for the study of tumor biology and for development of therapies against this highly lethal neoplasm.

Although GBM and MB comprise common malignant brain tumors, the catalogue of human brain tumors is extensive, and the richness of cell varieties in the CNS is reflected in the many varieties of brain tumors observed in the human population. Previous reports demonstrate that NSCs in the forebrain and hindbrain show developmental restrictions based on the brain regions from which they were derived (Klein et al., 2005; Merkle et al., 2007). The murine tumors described here showed striking similarities with specific subtypes of human brain tumors, suggesting a pathogenic role for MYCN in a heterogeneous group of human brain tumors. Together with the recently published models of MYC-driven MB (Kawauchi et al., 2012; Pei et al., 2012) we have recapitulated the most aggressive MYC/MYCN-driven human childhood brain tumors.

EXPERIMENTAL PROCEDURES

Animals and Bioluminescent Imaging

Generation of GTML mice of the FVB/NJ strain has been previously described (Swartling et al., 2010). Tumor progression of doubly *Glt1*-tTA/*MYCN*-TRE transgenic mice was continuously followed by luciferase signaling using the IVIS Lumina (Caliper Life Sciences, Mountain View, CA) using Living Image 2.5 software (Caliper Life Sciences, Mountain View, CA). Mice were injected with 75 mg/kg of sodium luciferin (LUCNA, Gold Biotechnology, St. Louis, MO) in saline prior to imaging. The mice selected for tumor removal and neurobasal cell culture all had high scores ($>5.0\times10^{10}$ photons/cm^2 sec) from bioluminescence imaging suggesting a functional bi-directional transgene expressing luciferase as previously reported (Swartling et al., 2010). For cell fate experiments *Glt1*-tTA mice were crossed with TRE-Cre:R26R-LSL-LacZ mice obtained from Dr. Robert Blelloch, UCSF. The *G-tva* mice has been described before (Holland and Varmus, 1998) and were generously provided by Dr. Eric Holland and backcrossed at least 5 generations into FVB/NJ strain before experimental use. Athymic Nude-Foxn1nu mice were obtained by Simonsen Laboratories (Gilroy, CA) or Harlan Laboratories (Venray, The Netherlands) and used in experimental procedures as described below. Mice were maintained in the Animal Facilities at University of California, San Francisco and at Uppsala University, Uppsala. All animal procedures were performed in accordance with national guidelines and regulations and approved by the Institutional Animal Care and Use Committee of the University of California in San Francisco and Uppsala Ethical Committee on Animal Experiments in Uppsala.

Neural stem/progenitor cell and tumor cell culturing

Normal tissue or part of tumor was removed and mechanically dissolved in cold Hanks buffer without Calcium and Magnesium (Cell Culture Facility, UCSF, Mission Bay, San Francisco). After one more wash in cold Hanks buffer sample was incubated 20 minutes in activated papain (Worthington, Lakewood, NJ). Tumor cells were gently dissociated and

cultured in neurobasal media (Gibco) without Vitamin A, supplemented with antibiotics (Cell Culture Facility, UCSF), B27 without Vitamin A (Invitrogen), L-glutamine and 20ng/ml EGF (Sigma) and 20ng/ml FGF-2 ((Peprotech, Rocky Hill, NJ, USA)). Cells were cultured and propagated on low adhesion plates (Corning) for 1 week, further passaged and used in experiments. SVZ neurospheres were established from FVB/N WT mice and similarly cultured as described above. Forebrains of E16.5 (described as E16) and P0.5 (described as P0) were coronally sectioned (100 μm thick sections) and sections 2.5–3.5 mm posterior of the base of olfactory bulb (OB) and the dorsal regions closest to the ventricles were isolated and dissociated as above. Total cerebellum was carefully removed excluding any parts of meninges, brain stem or midbrain, dissociated and similarly cultured as above. GNPs were enriched and cultured as previously described in 10ng/ml SHH-N (SHH N-terminal peptide, R&D Systems) containing serum-free media (Swartling et al., 2010).

Array Experiments

Expression analysis (as presented in Figure 5 and Figure S5) was performed on 103 primary human medulloblastoma using Affymetrix exon arrays as previously described (Northcott et al., 2009; Swartling et al., 2010). All tumor specimens were obtained in accordance with the Research Ethics Board at the Hospital for Sick Children (Toronto, Canada) and de-identified prior to analyses (Northcott et al. 2009). We studied the expression levels of SOX9, MYCN, MATH1, OLIG2 and NGN1 in four distinct molecular variants described as WNT, SHH, group C, and group D tumors as previously identified by multiple unsupervised analyses of these medulloblastoma samples (Northcott et al., 2010). RNA from tumors was isolated using Trizol (Invitrogen, Carlsbad, CA) and purified using the RNeasy Mini Kit (QIAGEN, Valencia, CA). For the GTML tumors, 1 μg of RNA was used as a starting template for the RiboMinus rRNA subtraction protocol (Invitrogen) followed by the ST labeling protocol (Affymetrix, Santa Clara, CA). For the transplanted tumors, 100 ng of RNA was used as a starting template for the Ambion WT Expression protocol (Applied Biosystems, Carlsbad, CA) followed by the WT Terminal Labeling protocol (Affymetrix). Labeled samples were hybridized to Affymetrix Mouse Exon 1.0 arrays. All arrays were normalized together with expression values calculated using RMA in the XPS package in R. Boxplots were generated in R using the standard graphics package. 2-way comparisons between groups were performed using Significance of Microarrays (SAM) (Tusher et al., 2001).

Supplementary Material

Refer to Web version on PubMed Central for supplementary material.

Acknowledgments

The authors would like to acknowledge Eric Holland, Anna-Marie Kenney and Daniel Fults for RCAS constructs, Monica Venere and Robert Blelloch for the TRE-Cre:R26R-LSL-LacZ transgene, Cynthia Cowdrey and the UCSF Brain Tumor Research Center Tissue Core for tumor samples, and Kim Nguyen and Slava Yakovenko for skillful technical assistance. We thank Jan Grawé and BioVIS, SciLifeLab at Uppsala University, for help with cell sorting. We thank David Rowitch and Richard Gilbertson for helpful discussions and Justin Meyerowitz for critical reading of the manuscript. We acknowledge support from the Pediatric Brain Tumor Foundation, the Swedish Research Council, the Swedish Cancer Society, the Swedish Childhood Cancer Foundation, Ake Wibergs Stiftelse, Lions Cancerforskningsfond, Stiftelsen Lars Hiertas Minne, Children's Brain Tumor Foundation, NIHR01 CA133091, CA148699, and CA159859. This work was also supported by funds from NIH K08 NS063456 to J.J.P and Hellmann Fellowship Award and the American Brain Tumor Association Translational Award to A.I.P.

References

1. Comprehensive genomic characterization defines human glioblastoma genes and core pathways. Nature. 455:1061–1068. [PubMed: 18772890]

2. Ahn S, Joyner AL. In vivo analysis of quiescent adult neural stem cells responding to Sonic hedgehog. Nature. 2005; 437:894–897. [PubMed: 16208373]
3. Akazawa C, Ishibashi M, Shimizu C, Nakanishi S, Kageyama R. A mammalian helix-loop-helix factor structurally related to the product of Drosophila proneural gene atonal is a positive transcriptional regulator expressed in the developing nervous system. J Biol Chem. 1995; 270:8730–8738. [PubMed: 7721778]
4. Alcock J, Sottile V. Dynamic distribution and stem cell characteristics of Sox1-expressing cells in the cerebellar cortex. Cell Res. 2009; 19:1324–1333. [PubMed: 19823196]
5. Bagheri-Fam S, Barrionuevo F, Dohrmann U, Gunther T, Schule R, Kemler R, Mallo M, Kanzler B, Scherer G. Long-range upstream and downstream enhancers control distinct subsets of the complex spatiotemporal Sox9 expression pattern. Dev Biol. 2006; 291:382–397. [PubMed: 16458883]
6. Brennan C, Momota H, Hambardzumyan D, Ozawa T, Tandon A, Pedraza A, Holland E. Glioblastoma subclasses can be defined by activity among signal transduction pathways and associated genomic alterations. PLoS One. 2009; 4:e7752. [PubMed: 19915670]
7. Browd SR, Kenney AM, Gottfried ON, Yoon JW, Walterhouse D, Pedone CA, Fults DW. N-myc can substitute for insulin-like growth factor signaling in a mouse model of sonic hedgehog-induced medulloblastoma. Cancer Res. 2006; 66:2666–2672. [PubMed: 16510586]
8. Charron J, Malynn BA, Fisher P, Stewart V, Jeannotte L, Goff SP, Robertson EJ, Alt FW. Embryonic lethality in mice homozygous for a targeted disruption of the N-myc gene. Genes Dev. 1992; 6:2248–2257. [PubMed: 1459450]
9. Cho YJ, Tsherniak A, Tamayo P, Santagata S, Ligon A, Greulich H, Berhoukim R, Amani V, Goumnerova L, Eberhart CG, et al. Integrative genomic analysis of medulloblastoma identifies a molecular subgroup that drives poor clinical outcome. J Clin Oncol. 2011; 29:1424–1430. [PubMed: 21098324]
10. de Bont JM, Kros JM, Passier MM, Reddingius RE, Sillevis Smitt PA, Luider TM, den Boer ML, Pieters R. Differential expression and prognostic significance of SOX genes in pediatric medulloblastoma and ependymoma identified by microarray analysis. Neuro Oncol. 2008; 10:648–660. [PubMed: 18577562]
11. Doetsch F, Caille I, Lim DA, Garcia-Verdugo JM, Alvarez-Buylla A. Subventricular zone astrocytes are neural stem cells in the adult mammalian brain. Cell. 1999; 97:703–716. [PubMed: 10380923]
12. Eberhart CG, Kratz J, Wang Y, Summers K, Stearns D, Cohen K, Dang CV, Burger PC. Histopathological and molecular prognostic markers in medulloblastoma: c-myc, N-myc, TrkC, and anaplasia. J Neuropathol Exp Neurol. 2004; 63:441–449. [PubMed: 15198123]
13. Ellison DW, Dalton J, Kocak M, Nicholson SL, Fraga C, Neale G, Kenney AM, Brat DJ, Perry A, Yong WH, et al. Medulloblastoma: clinicopathological correlates of SHH, WNT, and non-SHH/WNT molecular subgroups. Acta Neuropathol. 2011; 121:381–396. [PubMed: 21267586]
14. Farah MH, Olson JM, Sucic HB, Hume RI, Tapscott SJ, Turner DL. Generation of neurons by transient expression of neural bHLH proteins in mammalian cells. Development. 2000; 127:693–702. [PubMed: 10648228]
15. Gibson P, Tong Y, Robinson G, Thompson MC, Currle DS, Eden C, Kranenburg TA, Hogg T, Poppleton H, Martin J, et al. Subtypes of medulloblastoma have distinct developmental origins. Nature. 2010; 468:1095–1099. [PubMed: 21150899]
16. Hatton BA, Knoepfler PS, Kenney AM, Rowitch DH, de Alboran IM, Olson JM, Eisenman RN. N-myc is an essential downstream effector of Shh signaling during both normal and neoplastic cerebellar growth. Cancer Res. 2006; 66:8655–8661. [PubMed: 16951180]
17. Holland EC, Celestino J, Dai C, Schaefer L, Sawaya RE, Fuller GN. Combined activation of Ras and Akt in neural progenitors induces glioblastoma formation in mice. Nat Genet. 2000; 25:55–57. [PubMed: 10802656]
18. Holland EC, Varmus HE. Basic fibroblast growth factor induces cell migration and proliferation after glia-specific gene transfer in mice. Proc Natl Acad Sci U S A. 1998; 95:1218–1223. [PubMed: 9448312]

19. Huang X, Liu J, Ketova T, Fleming JT, Grover VK, Cooper MK, Litingtung Y, Chiang C. Transventricular delivery of Sonic hedgehog is essential to cerebellar ventricular zone development. Proc Natl Acad Sci U S A. 2010; 107:8422–8427. [PubMed: 20400693]
20. Hui AB, Lo KW, Yin XL, Poon WS, Ng HK. Detection of multiple gene amplifications in glioblastoma multiforme using array-based comparative genomic hybridization. Lab Invest. 2001; 81:717–723. [PubMed: 11351043]
21. Johnson RA, Wright KD, Poppleton H, Mohankumar KM, Finkelstein D, Pounds SB, Rand V, Leary SE, White E, Eden C, et al. Cross-species genomics matches driver mutations and cell compartments to model ependymoma. Nature. 2010; 466:632–636. [PubMed: 20639864]
22. Kawauchi D, Robinson G, Uziel T, Gibson P, Rehg J, Gao C, Finkelstein D, Qu C, Pounds S, Ellison DW, et al. A mouse model of the most aggressive subgroup of human medulloblastoma. Cancer Cell. 2012; 21:168–180. [PubMed: 22340591]
23. Kessler JD, Hasegawa H, Brun SN, Yang ZJ, Dutton JW, Wang F, Wechsler-Reya RJ. N-myc alters the fate of preneoplastic cells in a mouse model of medulloblastoma. Genes Dev. 2009; 23:157–170. [PubMed: 19171780]
24. Klein C, Butt SJ, Machold RP, Johnson JE, Fishell G. Cerebellum- and forebrain-derived stem cells possess intrinsic regional character. Development. 2005; 132:4497–4508. [PubMed: 16162650]
25. Knoepfler PS, Cheng PF, Eisenman RN. N-myc is essential during neurogenesis for the rapid expansion of progenitor cell populations and the inhibition of neuronal differentiation. Genes Dev. 2002; 16:2699–2712. [PubMed: 12381668]
26. Kool M, Koster J, Bunt J, Hasselt NE, Lakeman A, van Sluis P, Troost D, Meeteren NS, Caron HN, Cloos J, et al. Integrated genomics identifies five medulloblastoma subtypes with distinct genetic profiles, pathway signatures and clinicopathological features. PLoS One. 2008; 3:e3088. [PubMed: 18769486]
27. Korshunov A, Remke M, Kool M, Hielscher T, Northcott PA, Williamson D, Pfaff E, Witt H, Jones DT, Ryzhova M, et al. Biological and clinical heterogeneity of MYCN-amplified medulloblastoma. Acta Neuropathol. 2011
28. Lee A, Kessler JD, Read TA, Kaiser C, Corbeil D, Huttner WB, Johnson JE, Wechsler-Reya RJ. Isolation of neural stem cells from the postnatal cerebellum. Nat Neurosci. 2005; 8:723–729. [PubMed: 15908947]
29. Ligon KL, Alberta JA, Kho AT, Weiss J, Kwaan MR, Nutt CL, Louis DN, Stiles CD, Rowitch DH. The oligodendroglial lineage marker OLIG2 is universally expressed in diffuse gliomas. J Neuropathol Exp Neurol. 2004; 63:499–509. [PubMed: 15198128]
30. Lin JC, Cai L, Cepko CL. The external granule layer of the developing chick cerebellum generates granule cells and cells of the isthmus and rostral hindbrain. J Neurosci. 2001; 21:159–168. [PubMed: 11150332]
31. Marino S, Vooijs M, van Der Gulden H, Jonkers J, Berns A. Induction of medulloblastomas in p53-null mutant mice by somatic inactivation of Rb in the external granular layer cells of the cerebellum. Genes Dev. 2000; 14:994–1004. [PubMed: 10783170]
32. Merkle FT, Mirzadeh Z, Alvarez-Buylla A. Mosaic organization of neural stem cells in the adult brain. Science. 2007; 317:381–384. [PubMed: 17615304]
33. Northcott PA, Fernandez LA, Hagan JP, Ellison DW, Grajkowska W, Gillespie Y, Grundy R, Van Meter T, Rutka JT, Croce CM, et al. The miR-17/92 polycistron is up-regulated in sonic hedgehog-driven medulloblastomas and induced by N-myc in sonic hedgehog-treated cerebellar neural precursors. Cancer Res. 2009; 69:3249–3255. [PubMed: 19351822]
34. Northcott PA, Korshunov A, Witt H, Hielscher T, Eberhart CG, Mack S, Bouffet E, Clifford SC, Hawkins CE, French P, et al. Medulloblastoma Comprises Four Distinct Molecular Variants. J Clin Oncol. 2010
35. Northcott PA, Korshunov A, Witt H, Hielscher T, Eberhart CG, Mack S, Bouffet E, Clifford SC, Hawkins CE, French P, et al. Medulloblastoma comprises four distinct molecular variants. J Clin Oncol. 2011; 29:1408–1414. [PubMed: 20823417]

36. Palma V, Lim DA, Dahmane N, Sanchez P, Brionne TC, Herzberg CD, Gitton Y, Carleton A, Alvarez-Buylla A, Ruiz i Altaba A. Sonic hedgehog controls stem cell behavior in the postnatal and adult brain. Development. 2005; 132:335–344. [PubMed: 15604099]
37. Pei Y, Moore CE, Wang J, Tewari AK, Eroshkin A, Cho YJ, Witt H, Korshunov A, Read TA, Sun JL, et al. An Animal Model of MYC-Driven Medulloblastoma. Cancer Cell. 2012; 21:155–167. [PubMed: 22340590]
38. Perry A, Miller CR, Gujrati M, Scheithauer BW, Zambrano SC, Jost SC, Raghavan R, Qian J, Cochran EJ, Huse JT, et al. Malignant gliomas with primitive neuroectodermal tumor-like components: a clinicopathologic and genetic study of 53 cases. Brain Pathol. 2009; 19:81–90. [PubMed: 18452568]
39. Pfister S, Remke M, Benner A, Mendrzyk F, Toedt G, Felsberg J, Wittmann A, Devens F, Gerber NU, Joos S, et al. Outcome prediction in pediatric medulloblastoma based on DNA copy-number aberrations of chromosomes 6q and 17q and the MYC and MYCN loci. J Clin Oncol. 2009; 27:1627–1636. [PubMed: 19255330]
40. Polkinghorn WR, Tarbell NJ. Medulloblastoma: tumorigenesis, current clinical paradigm, and efforts to improve risk stratification. Nat Clin Pract Oncol. 2007; 4:295–304. [PubMed: 17464337]
41. Pomeroy SL, Tamayo P, Gaasenbeek M, Sturla LM, Angelo M, McLaughlin ME, Kim JY, Goumnerova LC, Black PM, Lau C, et al. Prediction of central nervous system embryonal tumour outcome based on gene expression. Nature. 2002; 415:436–442. [PubMed: 11807556]
42. Reynolds BA, Weiss S. Generation of neurons and astrocytes from isolated cells of the adult mammalian central nervous system. Science. 1992; 255:1707–1710. [PubMed: 1553558]
43. Salghetti SE, Kim SY, Tansey WP. Destruction of Myc by ubiquitin-mediated proteolysis: cancer-associated and transforming mutations stabilize Myc. EMBO J. 1999; 18:717–726. [PubMed: 9927431]
44. Salsano E, Croci L, Maderna E, Lupo L, Pollo B, Giordana MT, Consalez GG, Finocchiaro G. Expression of the neurogenic basic helix-loop-helix transcription factor NEUROG1 identifies a subgroup of medulloblastomas not expressing ATOH1. Neuro Oncol. 2007; 9:298–307. [PubMed: 17522332]
45. Schmitt A, Asan E, Puschel B, Jons T, Kugler P. Expression of the glutamate transporter GLT1 in neural cells of the rat central nervous system: non-radioactive in situ hybridization and comparative immunocytochemistry. Neuroscience. 1996; 71:989–1004. [PubMed: 8684627]
46. Schuller U, Heine VM, Mao J, Kho AT, Dillon AK, Han YG, Huillard E, Sun T, Ligon AH, Qian Y, et al. Acquisition of granule neuron precursor identity is a critical determinant of progenitor cell competence to form Shh-induced medulloblastoma. Cancer Cell. 2008; 14:123–134. [PubMed: 18691547]
47. Scott CE, Wynn SL, Sesay A, Cruz C, Cheung M, Gomez Gaviro MV, Booth S, Gao B, Cheah KS, Lovell-Badge R, Briscoe J. SOX9 induces and maintains neural stem cells. Nat Neurosci. 2010; 13:1181–1189. [PubMed: 20871603]
48. Stanton BR, Perkins AS, Tessarollo L, Sassoon DA, Parada LF. Loss of N-myc function results in embryonic lethality and failure of the epithelial component of the embryo to develop. Genes Dev. 1992; 6:2235–2247. [PubMed: 1459449]
49. Stolt CC, Lommes P, Sock E, Chaboissier MC, Schedl A, Wegner M. The Sox9 transcription factor determines glial fate choice in the developing spinal cord. Genes Dev. 2003; 17:1677–1689. [PubMed: 12842915]
50. Storm R, Cholewa-Waclaw J, Reuter K, Brohl D, Sieber M, Treier M, Muller T, Birchmeier C. The bHLH transcription factor Olig3 marks the dorsal neuroepithelium of the hindbrain and is essential for the development of brainstem nuclei. Development. 2009; 136:295–305. [PubMed: 19088088]
51. Sutter R, Shakhova O, Bhagat H, Behesti H, Sutter C, Penkar S, Santuccione A, Bernays R, Heppner FL, Schuller U, et al. Cerebellar stem cells act as medulloblastoma-initiating cells in a mouse model and a neural stem cell signature characterizes a subset of human medulloblastomas. Oncogene. 2010; 29:1845–1856. [PubMed: 20062081]

52. Swartling FJ, Ferletta M, Kastemar M, Weiss WA, Westermark B. Cyclic GMP-dependent protein kinase II inhibits cell proliferation, Sox9 expression and Akt phosphorylation in human glioma cell lines. Oncogene. 2009; 28:3121–3131. [PubMed: 19543319]

53. Swartling FJ, Grimmer MR, Hackett CS, Northcott PA, Fan QW, Goldenberg DD, Lau J, Masic S, Nguyen K, Yakovenko S, et al. Pleiotropic role for MYCN in medulloblastoma. Genes Dev. 2010; 24:1059–1072. [PubMed: 20478998]

54. Taipale J, Chen JK, Cooper MK, Wang B, Mann RK, Milenkovic L, Scott MP, Beachy PA. Effects of oncogenic mutations in Smoothened and Patched can be reversed by cyclopamine. Nature. 2000; 406:1005–1009. [PubMed: 10984056]

55. Taylor MD, Northcott PA, Korshunov A, Remke M, Cho YJ, Clifford SC, Eberhart CG, Parsons DW, Rutkowski S, Gajjar A, et al. Molecular subgroups of medulloblastoma: the current consensus. Acta Neuropathol. 2011

56. Thompson MC, Fuller C, Hogg TL, Dalton J, Finkelstein D, Lau CC, Chintagumpala M, Adesina A, Ashley DM, Kellie SJ, et al. Genomics identifies medulloblastoma subgroups that are enriched for specific genetic alterations. J Clin Oncol. 2006; 24:1924–1931. [PubMed: 16567768]

57. Tusher VG, Tibshirani R, Chu G. Significance analysis of microarrays applied to the ionizing radiation response. Proc Natl Acad Sci U S A. 2001; 98:5116–5121. [PubMed: 11309499]

58. Vidal VP, Chaboissier MC, Lutzkendorf S, Cotsarelis G, Mill P, Hui CC, Ortonne N, Ortonne JP, Schedl A. Sox9 is essential for outer root sheath differentiation and the formation of the hair stem cell compartment. Curr Biol. 2005; 15:1340–1351. [PubMed: 16085486]

59. Yang ZJ, Ellis T, Markant SL, Read TA, Kessler JD, Bourboulas M, Schuller U, Machold R, Fishell G, Rowitch DH, et al. Medulloblastoma can be initiated by deletion of Patched in lineage-restricted progenitors or stem cells. Cancer Cell. 2008; 14:135–145. [PubMed: 18691548]

Significance

Medulloblastoma (MB)/primitive neuroectodermal tumors (PNETs) and glioma represent the most common primary malignant brain tumors in children and adults. These tumors presumably arise from a population of cells that share with normal NSCs, a requirement for self-renewal and multi-lineage differentiation. *N-myc*, a proto-oncogene implicated in both normal brain development and brain tumors, induced a SHH-dependent program in normal NSCs derived from prenatal, and a SHH-independent program in NSCs derived from postnatal hindbrain. Orthotopic transplantation of *N-myc*-transduced NSCs generated MB/PNETs from hindbrain NSCs, and glioma from forebrain NSCs. Thus, the diversity of brain tumors in patients may be controlled by a limited set of transcription factors, reflecting both regional and temporal developmental restrictions among normal NSCs.

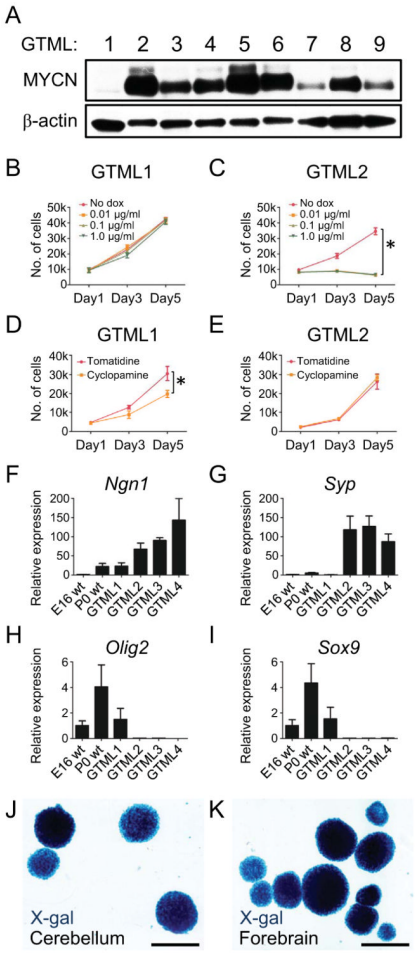

Figure 1. GLT1 drives *MYCN*-dependent, predominantly SHH-negative medulloblastoma and is a fate determinant for NSCs

(A) Immunoblot of MYCN in GTML MB spheres (passages 6–10).

(B–C) Proliferation of MYCN-low (GTML1) and MYCN-high (GTML2) spheres as indicated.

(D–E) All GTML sphere lines except GTML1 were insensitive to the SMO inhibitor cyclopamine (5μM). Tomatidine, 5μM, was used as control.

(F–I) Relative expression of neuronal markers Ngn1 and Syp; and Olig2 and Sox9 that are expressed in glial cells in embryonic (E16 WT), and postnatal (P0 WT) normal neurospheres and tumor spheres GTML1-4.

(J–K) GLT1-positive origin shown by X-gal fate mapping in NSCs isolated from postnatal (P0) cerebellum and postnatal (P0) forebrain from a *Glt1*-tTA; TRE-Cre-Rosa26-LSL-LacZ mouse.

Error bars: +/− Standard Deviation (SD). Scale: 100μm. See also Figure S1.

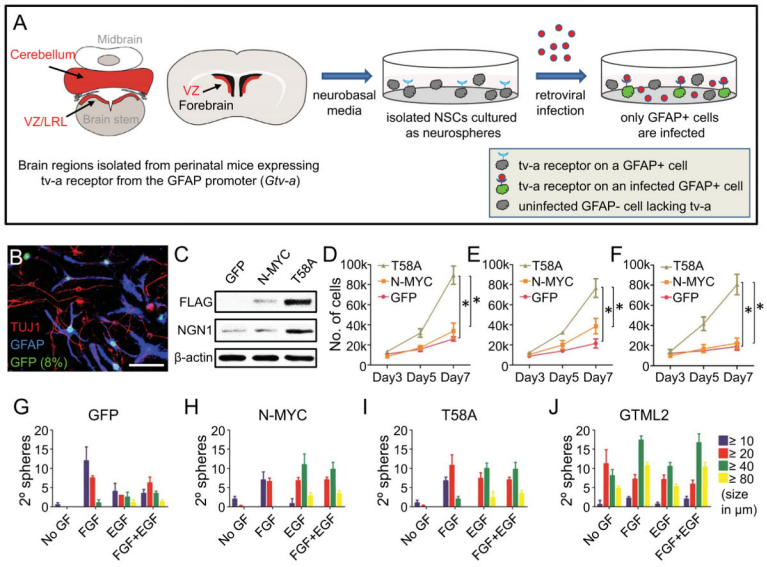

Figure 2. NSC-selective infection with *N-myc*^{T58A} alters proliferation and differentiation

(A) NSCs isolated from E16 and P0 forebrain (ventricular zone), E16 and P0 hindbrain (total cerebellum) and E14, E16 and P0 brain stem (ventricular zone/lower rhombic lip) from mice transgenic for *Gtv-a* were cultured for 7d in NB media on low-affinity plates with one or two passages. RCAS viruses containing GFP, *N-myc*^{WT} (N-MYC) or *N-myc*^{T58A} (T58A) came from supernatants of DF-1 virus producing cells (see Figure S2). NSCs were transduced with RCAS viruses mixed 1:1 with fresh NB media. Cells were infected (72h), dissociated and cultured in fresh NB media. Cells were orthotopically transplanted in nude mice 7 days after RCAS infection.

(B) Selective infection of GFAP-positive P0 cerebellar NSCs, evidenced by co-expression of RCAS-GFP (green) with GFAP (blue) 72h after growth factor depletion. TUJ1 (red). Scale: 25 μm.

(C) Immunoblot of FLAG-tagged *N-myc*^{WT} or *N-myc*^{T58A} in P0 cerebellar NSCs. NGN1 and β-actin control are also shown.

(D–F) Proliferation at 3, 5 and 7 days after transduction with GFP, *N-myc*^{WT} or *N-myc*^{T58A} of P0 NSCs isolated from cerebellum (D), forebrain (E) and dorsal brain stem/lower rhombic lip (F) respectively.

(G–J) Growth factor independence assay showing sphere diameter (as indicated) and number of secondary spheres in P0 cerebellar NSCs transduced with GFP, *N-myc*^{WT} or *N-myc*^{T58A} and in GTML2 spheres. Although not indicated, there are significantly more spheres irrespective of size in “GF conditions” (FGF, EGF or FGF+EGF) as compared to “no GF conditions” when analyzing GFP-, N-MYC- and T58A-transduced NSCs, respectively, when using Student’s *t*-test ($p < 0.05$).

Error bars: +/− SD. See also Figure S2.

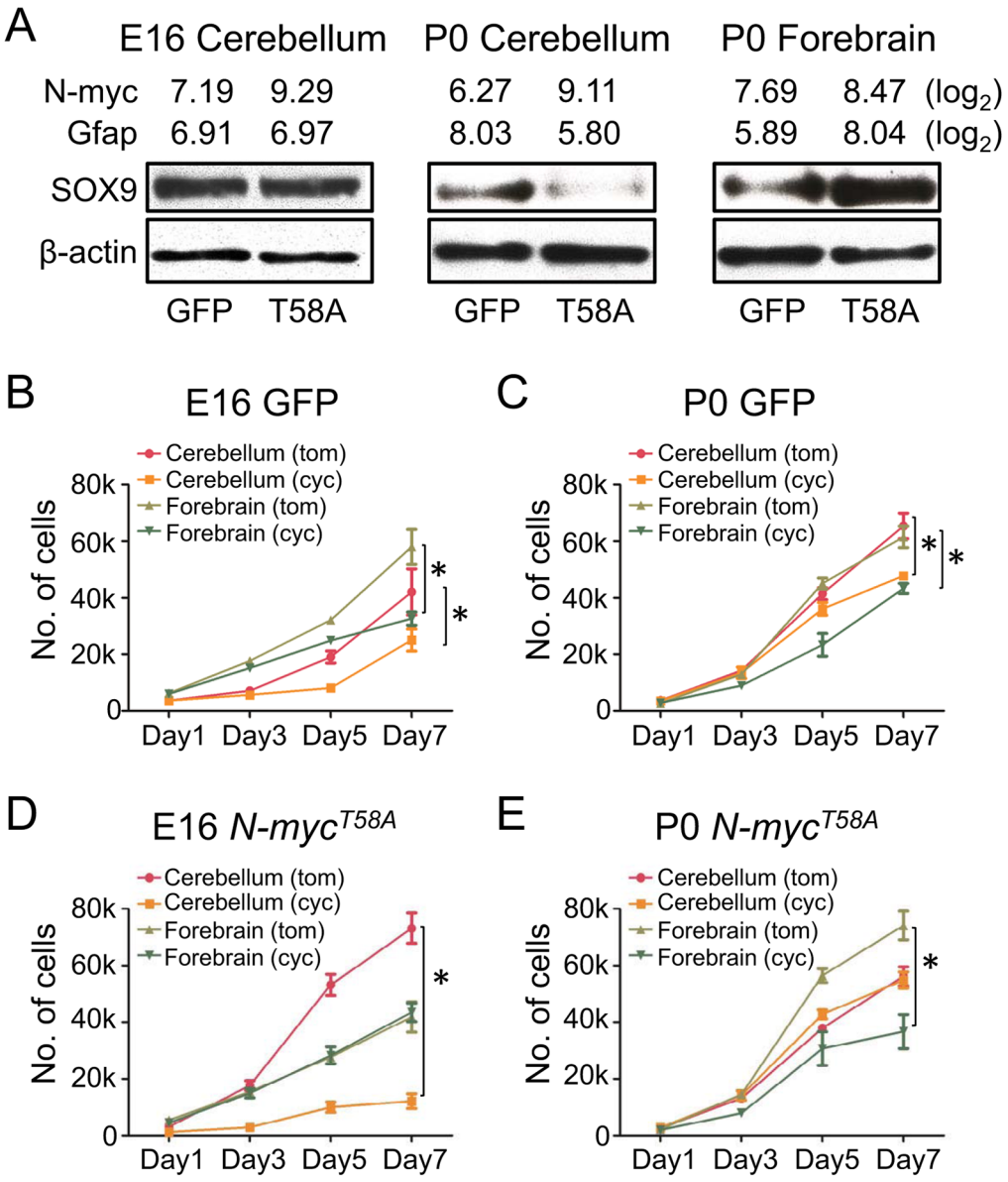

Figure 3. The *N-myc*^{T58A}-driven neuronal program depends on regional origin and NSC age

(A) Levels of N-myc and Gfap from Affymetrix exon arrays (log_2 values) and immunoblots of SOX9 and β-actin in E16 and P0 cerebellar and P0 forebrain NSCs transduced with GFP or *N-myc*^{T58A}, respectively.

(B–E) Proliferation (7 days) of cerebellar and forebrain NSCs transduced with GFP (B–C) or *N-myc*^{T58A} (D–E) and treated with cyclopamine (cyc) or tomatidine (tom) in 5μM final concentrations for E16 and P0 ages, respectively.

Error bars: +/− SD. * indicates $p < 0.05$ from Student's *t*-test. See also Figure S3.

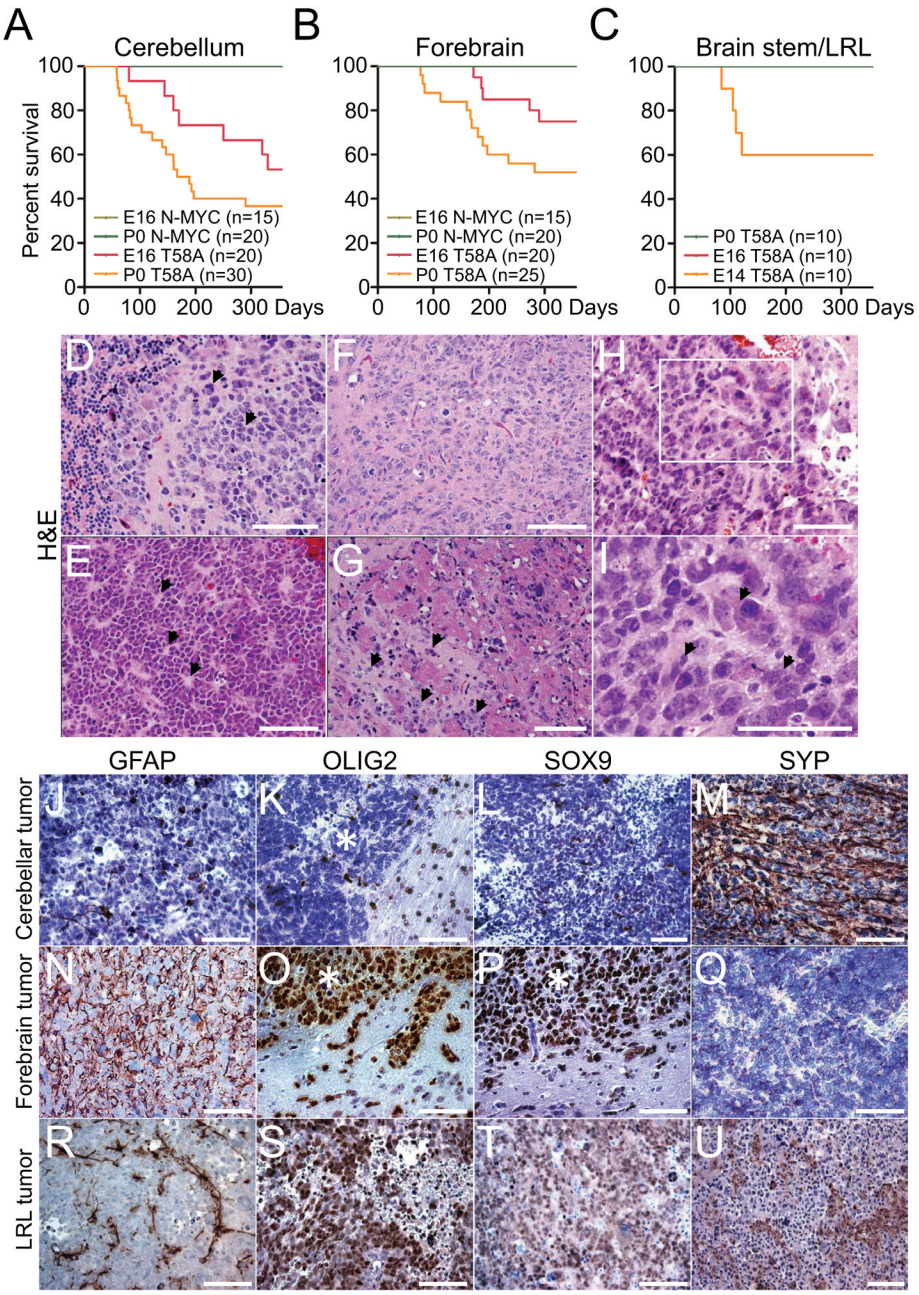

Figure 4. *N-myc*^{T58A} induces brain tumors from both cerebellum and forebrain

(A–C) Survival of mice orthotopically transplanted with 100,000 NSCs isolated from forebrain, cerebellum and brain stem/LRL, transduced with *N-myc*^{WT} or *N-myc*^{T58A} viruses. n=number of mice per group. Mice injected with *N-myc*^{WT} NSCs (green colors) or *N-myc*^{T58A} E16 and P0 brain stem/LRL (red and green, respectively) generated no tumors. (D–I) Histopathology of representative P0 cerebellar (D and E), P0 forebrain (F and G), and E14 brain stem/LRL (H–I) *N-myc*^{T58A} tumors (H&E staining). Cerebellar tumors displayed MB features, including cell wrapping in a tumor with prominent LC/A features (D, arrowhead) and Homer Wright rosettes (E, arrowhead). Forebrain tumors displayed diffuse invasion of tumor cells along white matter tracts (arrowhead) (G). LRL tumors displayed

marked cellular and nuclear pleomorphism (I, arrowhead). Box in H (200x) denotes region shown at higher magnification in I (400x).
(J–U) Immunostaining, of representative *N-myc*^{T58A}-induced cerebellar, forebrain, and LRL tumors demonstrating greater neuronal differentiation in cerebellar tumors, greater glial differentiation in forebrain tumors, and intermediate differentiation in LRL tumors. * indicate tumor region in pictures where an adjacent normal brain is present.
Scale: 100μm. See also Figure S4 and Table S1.

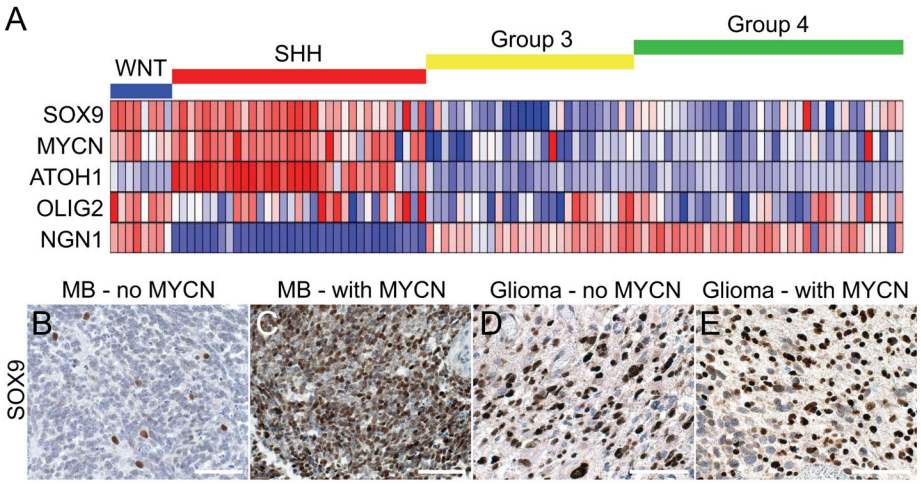

Figure 5. SOX9 marks a SHH-dependent brain tumor profile

(A) Expression analysis of 103 primary MB samples clustered in four MB subgroups, WNT, SHH, Group 3 and Group 4 with levels normalized to normal adult cerebella (n=5) as described previously (Northcott et al., 2011). Dark blue represents the lowest and dark red the highest expression.

(B–E) SOX9 immunostaining in representative human MB (B and C) and glioma (D and E) sections, without and with *MYCN* amplification, as determined by fluorescent in situ hybridization (Perry et al., 2009).

Scale: 100μm. See also Figure S5 and Table S2.

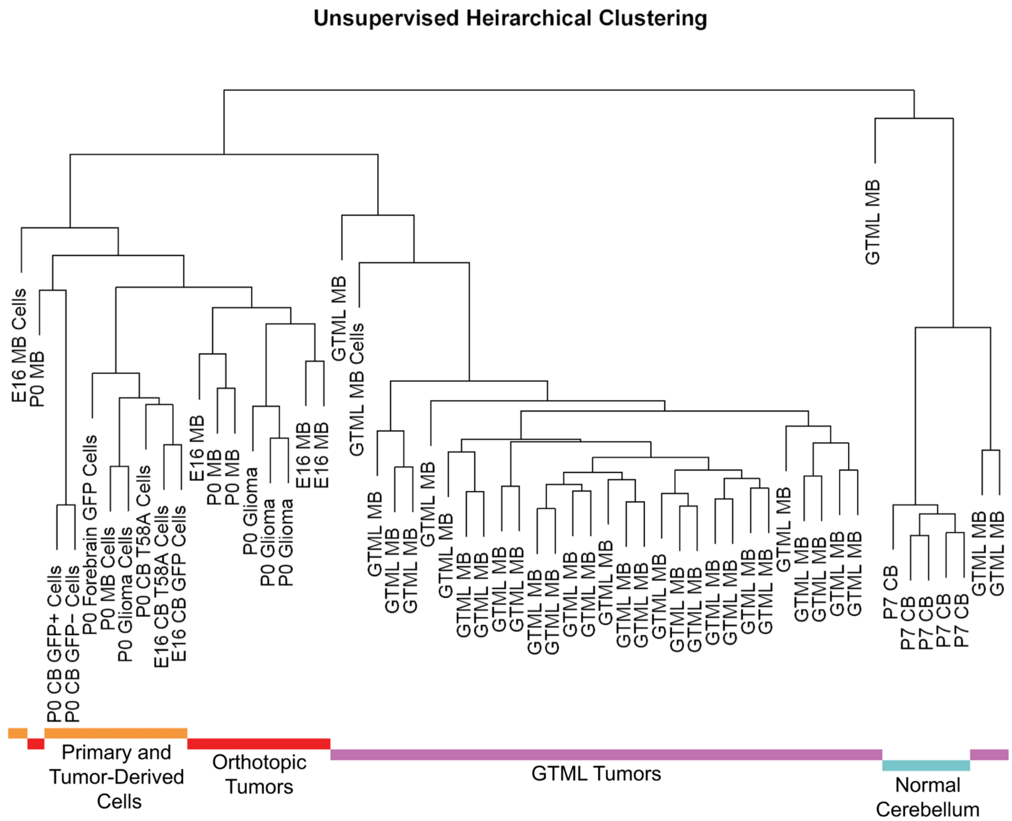

Figure 6. *N-myc*^{T58A} tumors, GTML tumors, and normal murine tissues show discrete expression signatures

Dendrogram showing unsupervised hierarchical clustering from Affymetrix exon array data obtained from: (1) Primary and Tumor-Derived Cells (yellow): Four individual GFP-transduced E16 and P0 cerebellar (sorted or unsorted for GFP-infection using cell sorting) NSCs, P0 forebrain NSCs, two *N-myc*^{T58A}-transduced E16 and P0 cerebellar NSCs (in low passages) and three cell lines (in low passages) derived from orthotopic E16 and P0 cerebellar and P0 forebrain tumors. (2) Orthotopic Tumors (red): Nine freshly isolated orthotopic E16 and P0 cerebellar and P0 forebrain *N-myc*^{T58A}-tumors. (3) GTML Tumors (purple): 32 isolated GTML tumors and one cultured GTML tumor cell line (GTML2). (4) Normal Cerebellum (blue): Four samples from P7 GTML double heterozygous total cerebella. The distance in the clustering determines how well samples are related to each other. See also Figure S6.

NIH-PA Author Manuscript
NIH-PA Author Manuscript

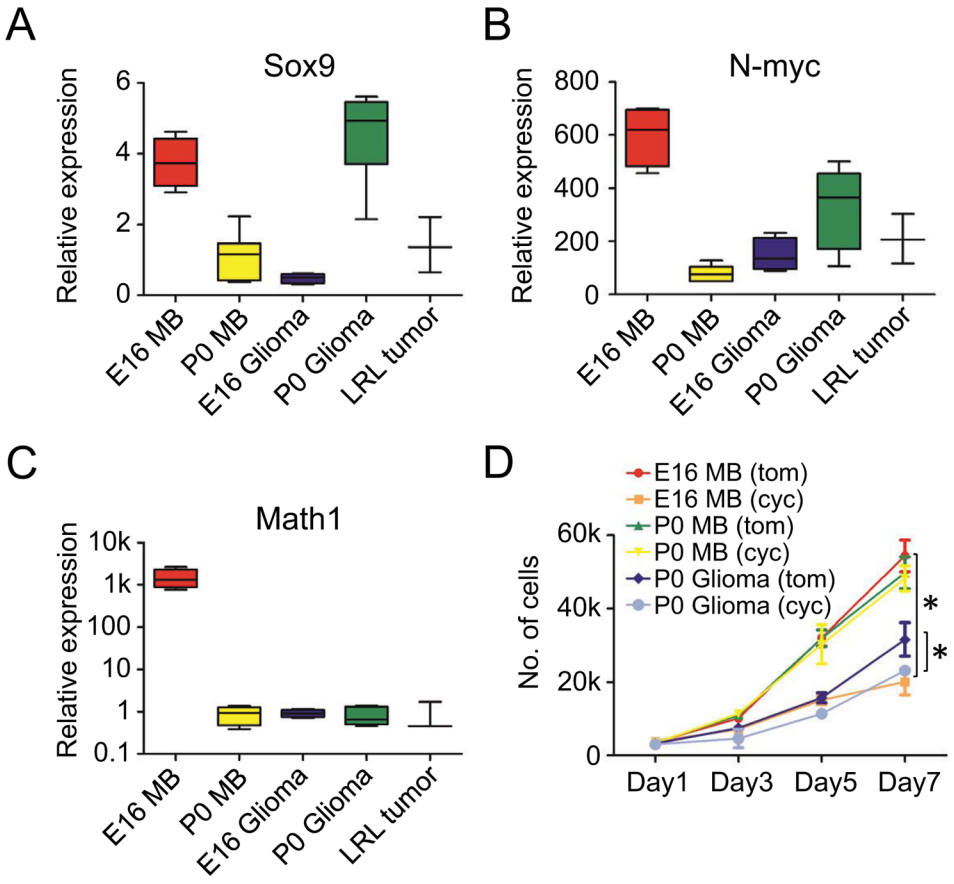

Figure 7. N-MYC drives both SHH-dependent and SHH-independent MB

(A–C) Relative expression of Sox9, N-myc and Math1 in five disparate N-MYC-driven murine tumors, E16 MB (n=4), P0 MB (n=6), E16 glioma (n=4), P0 glioma (n=6) and E14 LRL tumor (n=3). n=number of individual tumors. Boxes are the first to third quartile with the median indicated. No boxes are shown for LRL tumors because of few samples (n=3). Whiskers go from min to max values.

(D) Proliferation of cultures of E16 MB, P0 MB and P0 glioma isolated from individual tumors and treated with cyclopamine (cyc) or tomatidine (tom) used at final concentrations of 5μM. * indicates statistical significance ($p < 0.05$) from Student's *t*-test. Error bars: +/− SD.

See also Figure S7 and Table S3.

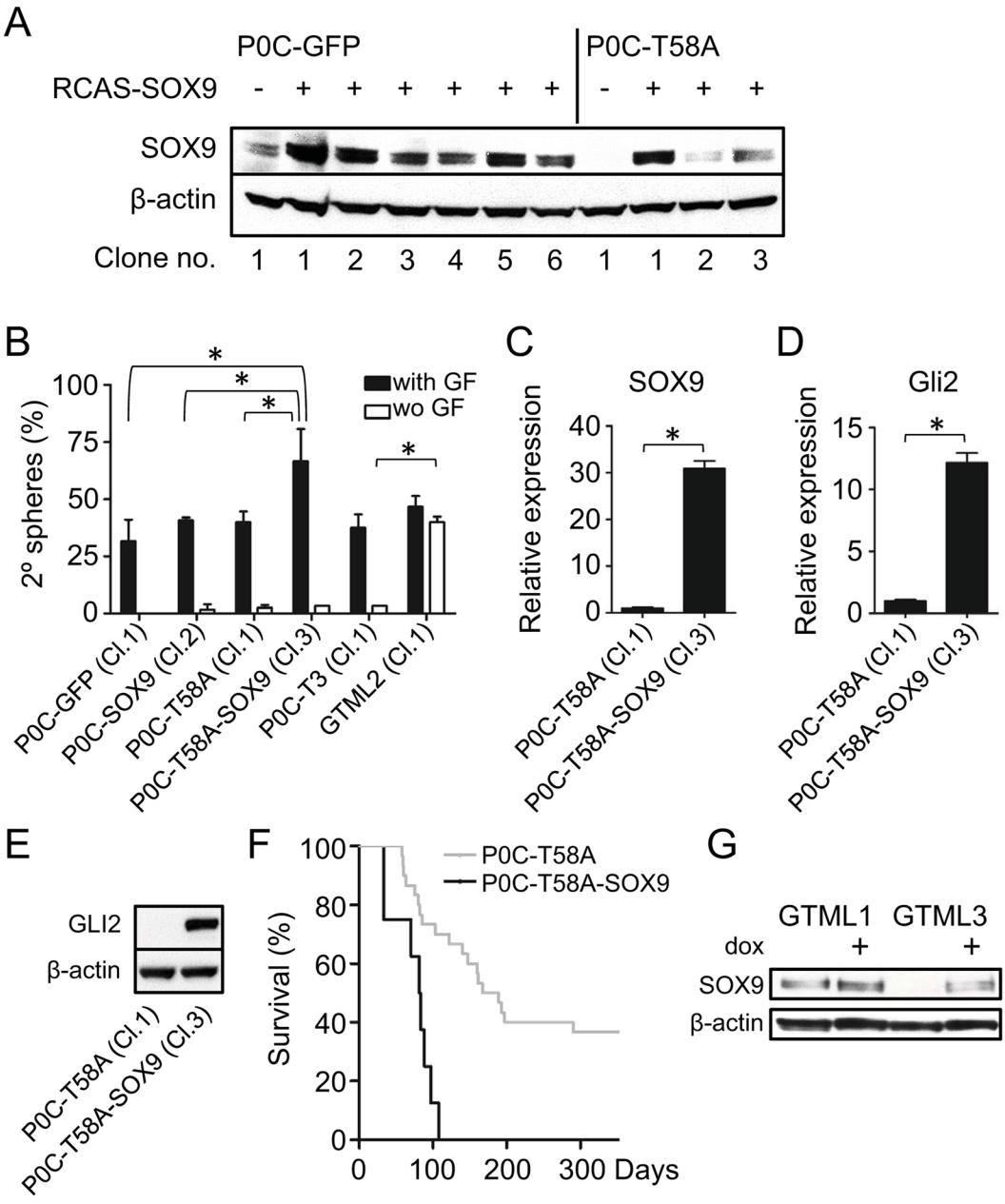

Figure 8. SOX9 promotes self-renewal and N-MYC-driven brain tumor incidence

(A) Immunoblot of NSCs generated from single cells of GFP- and SOX9-transduced P0 cerebellar NSCs from normal (six individual clones) and *N-myc*^{T58A} transduced NSCs (three individual clones).

(B) Limiting dilution assay showing secondary (2°) spheres cultured starting from one single cell per well (with or without (wo) EGF and FGF). Numbers indicates mean values (from two experiments) of spheres per well from a total of 60 wells counted (shown as %). Clone numbers used (from A) are indicated. Assay results from single clones from a P0 MB tumor (P0C-T3 (Cl.1)) and from a GTML tumor (GTML2 (Cl.1)) are also included. * indicates statistical significance ($p < 0.05$) from Student's *t*-test.

(C–D) Relative expression of SOX9 and Gli2 in *N-myc*^{T58A}-transduced P0 cerebellar NSCs and *N-myc*^{T58A}-transduced P0 cerebellar NSCs further transduced with SOX9 (P0C-T58A-SOX9 Cl.3), respectively. For SOX9 expression and clone numbers, see A. * indicates statistical significance ($p < 0.05$) from Student's *t*-test.
(E) Immunoblot showing GLI2 protein expression in *N-myc*^{T58A}-transduced P0 cerebellar normal (P0C-T58A Cl.1) or SOX9-transduced (P0C-T58A-SOX9 Cl.3) clones.
(F) Survival after orthotopic transplantation of 100,000 cells from *N-myc*^{T58A} P0 cerebellar NSCs (P0C-T58A, as used in Figure 4A; n=30) and *N-myc*^{T58A} P0 cerebellar NSCs further transduced with SOX9 (P0C-T58A-SOX9, n=10), respectively. Same clone (Cl.3) was used as in C–E.
(G) Re-expression of SOX9 in representative GTML spheres (GTML3) treated with dox (1μg/ml) after 72h as shown in an immunoblot, with GTML1 cells as controls. * indicates statistical significance ($p < 0.05$) from Student's *t*-test.
Error bars: +/− SD. See also Figure S8.